

基于两性离子配体构筑的Eu(III)配位聚合物的 晶体结构和对呋喃西林的检测

王凯民¹ 李立凤¹ 石明凤¹ 叶艳青^{*1} 王玉娜^{*2} 郭津榕¹ 唐怀军¹ 马钰璐^{*2}

(¹云南民族大学化学与环境学院,昆明 650504)

(²昆明医科大学药学院暨云南省天然药物药理重点实验室,昆明 650500)

摘要: 合成了一个新的铕(III)配合聚合物 $\{[\text{Eu}(\text{L})_2(\text{H}_2\text{O})_4]\text{Cl}_3 \cdot 2\text{H}_2\text{O}\}_n$ (**1**) (L=1,1'-(2,3,5,6-四甲基-1,4-亚苯基)双(亚甲基)双(吡啶-1-鎓-4-羧酸盐))。配位聚合物分子结构经X射线单晶衍射分析确认。对配合物**1**进行了X射线粉末衍射、红外光谱、热重法和固体荧光光谱表征。固体荧光测试显示配合物**1**具有非常明显的稀土铕离子特征发光,表明配体能够高效地敏化稀土离子发光。此外,这种水稳定的**1**被用作化学传感器来检测各种常见的抗生素,发现它对水相中的呋喃西林分子表现出高选择性、高灵敏度和可循环的检测能力。

关键词: 铕(III)配合物; 配位聚合物; 两性离子配体; 荧光识别; 呋喃西林

中图分类号: O614.33*8 文献标识码: A 文章编号: 1001-4861(2022)09-1843-10

DOI: 10.11862/CJIC.2022.196

Crystal Structure of Eu(III) Coordination Polymer Based on Zwitterionic Ligand and Detection of Furacilin

WANG Kai-Min¹ LI Li-Feng¹ SHI Ming-Feng¹ YE Yan-Qing

WANG Yu-Na GUO Jin-Rong¹ TANG Huai-Jun¹ MA Yu-Lu^{*2}

(¹School of Chemistry & Environment, Yunnan Minzu University, Kunming 650504, China)

(²School of Pharmaceutical Sciences and Yunnan Key Laboratory of Pharmacology for
Natural Products, Kunming Medical University, Kunming 650500, China)

Abstract: A novel coordination polymer, $\{[\text{Eu}(\text{L})_2(\text{H}_2\text{O})_4]\text{Cl}_3 \cdot 2\text{H}_2\text{O}\}_n$ (**1**) (L=1,1'-((2,3,5,6-tetramethyl-1,4-phenylene) bis(methylene))bis(pyridin-1-ium-4-carboxylate)), was synthesized under hydrothermal conditions by a zwitterionic organic ligand and characterized by single crystal X-ray diffraction. Powder X-ray diffraction, IR, thermogravimetry, and luminescence properties of **1** were also determined. The solid-state luminescence properties of **1** were investigated, realizing the zwitterionic ligand is an excellent antenna chromophore for sensitizing Eu^{3+} ions. In addition, this water-stable **1** was utilized as a chemosensor to detect various common antibiotics to find that this one can exhibit high selectivity, sensitivity, and recyclability in the detection of furacilin molecules in aqueous phases. CCDC: 2150460.

Keywords: Eu(III) complex; coordination polymer; zwitterionic ligand; fluorescence recognition; furacilin

收稿日期:2022-02-22。收修改稿日期:2022-08-01。

国家自然科学基金(No.21762049)、云南省科技厅基础研究基金(No.202001AU070111)、云南省科技厅昆明医科大学应用基础研究联合专项(No.202101AY070001-070)、云南省教育厅科学研究基金(No.2020J0140)和昆明市科技局基金(No.2020-1-H-035)资助。

*通信联系人。E-mail: yey-qing@163.com, kyyxywyn@163.com, yuluma163@163.com

0 Introduction

Coordination polymers (CPs), as a new multifunctional material, have attracted extensive attention of chemists not only because of their unique network structure but also rapid chromic behavior, including gas separation^[1], chemical catalysis^[2], magnetism^[3], optical properties^[4], biological application^[5], and so on^[6-10]. Compared with the conventional neutral ligands, the zwitterionic types of organic ligands have obvious advantages owing to their good solubility, improved adsorption selectivity of guest molecules, and strong coordination ability. However, to date, only limited CPs based on zwitterionic organic ligands have been demonstrated^[11-16]. Therefore, the CPs based on this class of ligands still need further exploration.

Furacilin is a synthetic antibiotic that can treat livestock diseases. It was widely used in animal husbandry and aquaculture a few years ago. Later, it was found that the residues of furacilin and the metabolites in animal-derived foods can be transmitted to humans through the food chain. Long-term intake of furacilin will cause various diseases and have side effects such as carcinogenesis and teratogenesis on the human body. The United States, Australia, Canada, Japan, Singapore, and the European Union have expressly prohibited the use of such drugs in the food industry, and strictly implemented the detection of nitrofurans residues in aquatic products. Furacilin is listed as a banned drug in China^[17-19]. Therefore, the development of new materials for the detection of furacilin is critical in terms of environmental considerations. Although various sophisticated methods^[20-22] such as GC-MS, LC-MS, and LC-UV have been developed for furacilin detection, these advanced analysis and testing techniques are limited by their inconvenient to carry, time-consuming and tedious operation, high cost, and not real-time monitoring drawbacks^[23-25]. Compared with the traditional detection methods, fluorescence detection based on complexes has the advantages of high sensibility, easy synthesis, low cost, and simple operation^[26].

In this work, a novel Eu(III) CP, $\{[\text{Eu}(\text{L})_2(\text{H}_2\text{O})_4]\text{Cl}_3 \cdot 2\text{H}_2\text{O}\}_n$ (**1**) (L=1,1'-(2,3,5,6-tetramethyl-1,4-phenylene)

bis(methylene))bis(pyridin-1-ium-4-carboxylate)), was synthesized under hydrothermal conditions by a zwitterionic organic ligand. X-ray diffraction analysis shows that **1** has a cationic skeleton on the main network and the Cl^- ions used to balance the charges just exist in its pores. Its structure, photoluminescence, and detection properties were systematically studied. Firstly, the solid-state luminescence properties of **1** were investigated, realizing the zwitterionic ligand is an excellent antenna chromophore for sensitizing Eu^{3+} ions. In addition, this water-stable **1** was utilized as a chemosensor to detect various common antibiotics to find that this one can exhibit high selectivity, sensitivity, and recyclability in the detection of furacilin molecules in aqueous phases.

1 Experimental

1.1 Materials and methods

All reagents used are commercially available analytical pure and can be used directly without purification. Powder X-ray diffraction (PXRD) was determined by a Bruker D8 Advance X-ray diffractometer ($\text{Cu } K\alpha$, $\lambda = 0.154\ 056\ \text{nm}$), in a 2θ range of $5^\circ - 50^\circ$, with a voltage of 35 kV and a current of 50 mA. Thermogravimetric analysis (TGA) was performed on a Perkin Elmer thermogravimetric analyzer from room temperature to $800\ ^\circ\text{C}$ with a heating rate of $10\ ^\circ\text{C} \cdot \text{min}^{-1}$ under an N_2 atmosphere. Elemental analyses (C, H, and N) were performed by an Elementar Vario EL III analyzer. The infrared spectrum was measured by the KBr tablet pressing method on FTS-400 Fourier transform spectrometer, with a wavelength range of $4\ 000 - 400\ \text{cm}^{-1}$. The UV spectrum was scanned by a Beijing Puxi TU-1901 double beam UV-Vis spectrophotometer. Solid and liquid fluorescence spectra were measured at room temperature using a HITACHI F-4500 fluorescence spectrophotometer.

1.2 Synthesis of CP 1

1,1'-(1,4-Phenylenebis(methylene))bis(4-carboxypyridin-1-ium) chloride ligand ($(\text{H}_2\text{L})\text{Cl}_2$, 0.02 mmol), $\text{EuCl}_3 \cdot 6\text{H}_2\text{O}$ solid (0.04 mmol), deionized water (2 mL), and methanol (1 mL) were added into a 10 mL beaker and mixed well. A NaOH aqueous solution ($0.01\ \text{mol} \cdot \text{L}^{-1}$) was added drop by drop to adjust the pH value of

the mixture to about 6. The mixture was stirred at room temperature for 30 min, then placed in a hydrothermal reactor and heated to 120 °C for 2 d. The mixture was cooled naturally to room temperature to obtain light yellow block crystals. The yield was 32.1% (based on (H₂L)Cl₂). Elemental analysis Calcd. for C₄₈H₆₀Cl₃EuN₄O₁₄(%): C, 49.05; H, 5.15; N, 4.77. Found (%): C, 48.76; H, 5.20; N, 4.74. IR (KBr, cm⁻¹): 3 423(br), 1 608(s), 1 564(s), 1 446(w), 1 384(s), 1 237(m), 1 120(m), 1 076(m), 1 042(m).

1.3 Crystal structure determination

Light colorless single crystals with a suitable quality of **1** were obtained under hydrothermal conditions. Crystallographic data for **1** were recorded on a Bruker APEX- II diffractometer with graphite monochromated Mo K α radiation (λ =0.071 073 nm) at 293(2) K using ω rotation scans. The crystal data was solved by direct

methods using the SHELXS program and refined by full - matrix least - squares on F^2 using SHELXS in Olex2 - 1.3 software^[27-29]. Non - hydrogen atoms were refined anisotropically. All hydrogen atoms were generated theoretically and were placed at geometrically estimated positions. The guest solvent molecules were disordered and not located, so the SQUEEZE method was added to the CIF file to remove the contributions of disordered guest molecules. The number of lattice water molecules and the final chemical formula of **1** were determined by combining the single-crystal structures and TGA results. The crystallographic data and structure refinement details of **1** are summarized in Table 1. The main bond lengths and bond angles for **1** are shown in Table 2 and the hydrogen bond parameters for **1** are listed in Table 3.

CCDC: 2150460.

Table 1 Crystal data and structure refinement of **1**

Parameter	1	Parameter	1
Formula	C ₄₈ H ₆₀ Cl ₃ EuN ₄ O ₁₄	<i>Z</i>	2
Formula weight	1 175.336	<i>D_c</i> / (g·cm ⁻³)	1.366
Crystal system	Monoclinic	μ / mm ⁻¹	1.335
Space group	<i>P2/c</i>	F(000)	1 164
<i>a</i> / nm	1.461 44(10)	Crystal size / mm	0.2×0.12×0.1
<i>b</i> / nm	1.098 32(6)	Reflection collected, unique	30 172, 7 511 (<i>R_{int}</i> =0.034 2)
<i>c</i> / nm	1.821 29(11)	GOF on F^2	1.052
β / (°)	108.595(7)	<i>R</i> ₁ , <i>wR</i> ₂ [<i>I</i> >2 σ (<i>I</i>)]	0.030 2, 0.084 5
<i>V</i> / nm ³	2.770 8(3)	<i>R</i> ₁ , <i>wR</i> ₂ (all data)	0.035 6, 0.086 8

Table 2 Selected bond lengths (nm) and bond angles (°) for **1**

Eu1—O1	0.243 9(15)	Eu1—O1a	0.243 9(15)	N1—C4	0.134 5(2)
Eu1—O2	0.241 9(19)	Eu1—O2a	0.241 9(19)	C1—C2	0.153 0(3)
Eu1—O3	0.239 1(15)	Eu1—O3a	0.239 1(15)		
Eu1—O4	0.242 4(17)	C1—O1	0.125 9(3)		
O1A—Eu1—O1	150.16(8)	O2a—Eu1—O2	74.17(11)	C1—O1—Eu1	132.69(14)
O2—Eu1—O1	72.93(6)	O2—Eu1—O4a	113.39(8)	N2—C18—C11	114.03(17)
O2—Eu1—O1a	134.79(6)	N1—C5—C6	120.43(18)		
O2A—Eu1—O1	134.78(6)	C4—N1—C5	120.71(17)		

Symmetry code: a: $-x, y, -z+1/2$.

Table 3 Hydrogen bond parameters for **1**

D—H···A	<i>d</i> (D—H) / nm	<i>d</i> (H···A) / nm	<i>d</i> (D···A) / nm	\angle DHA / (°)
C4—H4···Cl2	0.093	0.273	0.344 1(3)	134
C5—H5···Cl1	0.093	0.280	0.352 8(2)	136

Continued Table 3

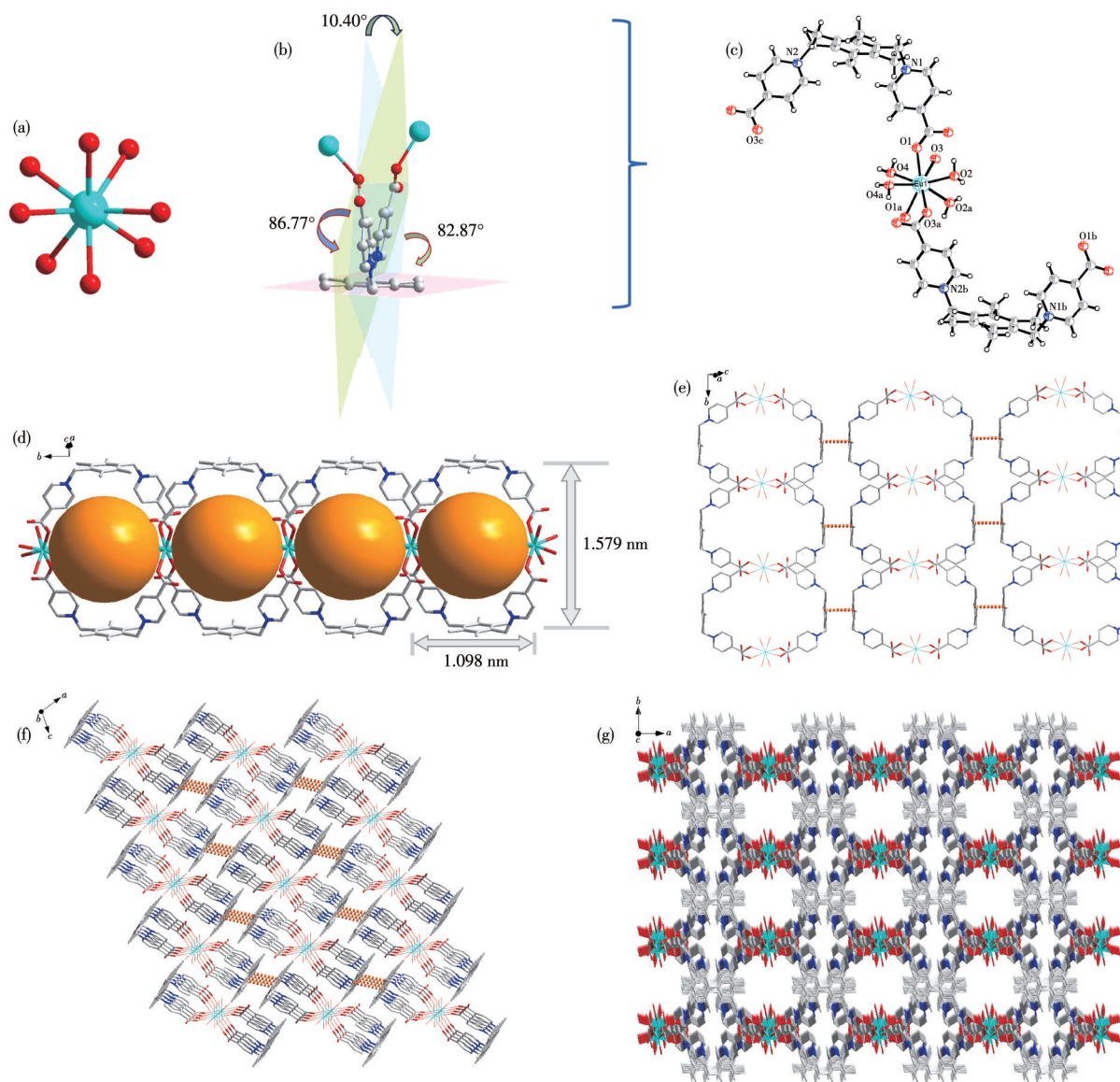
C7—H7A...Cl1	0.097	0.266	0.354 0(2)	151
C16—H16A...Cl1	0.096	0.276	0.365 9(3)	157
C19—H19...Cl2	0.093	0.280	0.351 6(3)	135

2 Results and discussion

2.1 Crystal structure of CP 1

Single-crystal X-ray diffraction measurement displays that CP **1** crystallizes in the monoclinic space group $P2_1/c$. As shown in Fig. 1c, the asymmetric unit consists of a crystallographically independent Eu(III) ion, two fully deprotonated linker L, four coordinated

water molecules, and three free Cl^- ions. The distorted guest solvent molecules in **1** were subtracted by the SQUEEZE method in the PLATON program. Each Eu(III) center is eight-coordinated to four O atoms (O1, O3, O1a, and O3a) of four L ligands and four O atoms (O2, O4, O2a, and O4a) of four water molecules, forming the primary building unit $[\text{EuO}_8]$ (Fig. 1a). The two



Guest species are omitted for clarity; Symmetry codes: a: $-x, y, -z+1/2$; b: $-x, y+1, -z+1/2$; c: $x, y-1, z$

Fig.1 Structure of CP **1**: (a) $[\text{EuO}_8]$ primary building unit of **1**; (b) coordination mode of L; (c) coordination environment; (d) 1D chain structure; (e) $\pi \cdots \pi$ stacking interactions; (f, g) overviewing of 3D packing plot

carboxylic acid groups of the zwitterionic ligand (H_2L) Cl_2 in **1** are completely deprotonated, forming two carboxylate groups which adopt the monodentate bridging mode ($\mu_1\text{-}\eta^1$) to coordinate to Eu(III) centers. Due to the presence of freely rotatable methylene ($\text{—CH}_2\text{—}$), the two pyridine rings rotate to the same side of the benzene ring, making each L ligand presents a concave shape. It should be noted that the dihedral angles produced between the benzene ring and the two pyridine rings are slightly different, which are 82.87° and 86.77° respectively. Besides, the two pyridine rings are not in the same plane, but are distributed at a dihedral angle of 10.40° (Fig. 1b). Adjacent $[\text{EuO}_8]$ building units are connected by two L ligands in opposite orientations, getting a hexagonal cage containing two L ligands and two Eu(III) centers. The $[\text{EuO}_8]$ vertex-sharing channels expand into a 1D bead chain extending along the b -axis with an effective pore size of $1.098\text{ nm}\times 1.579\text{ nm}$ (Fig. 1d). Then, through the $\pi\cdots\pi$ stacking interactions between neighboring benzene rings (centroid-centroid: 0.373 82 nm), the mutually parallel 1D bead chains are unfolded into a 2D layer on the $(10\bar{1})$ plane (Fig. 1e). Adjacent layers are further connected by the $\text{C—H}\cdots\text{Cl}$ hydrogen-bonding interactions between phenylmethyl groups and the free Cl^- ions to give a 3D supramolecular network (Fig. 1f and 1g). It should be pointed out that the L molecules used to form **1** are pyridinium zwitterionic ligands with dispersed positive and negative charge centers. The positive charges of the L molecule are mainly concentrated on the N atoms of the pyridine rings, and the negative charges are mainly centralized on the O atoms of the carboxylate groups. Therefore, **1** continues this characteristic of L, and its final structure also has separate charge centers. Interestingly, the negative charges of the carboxylate groups are neutralized by the Eu(III) ions, so the main skeleton of **1** is positively charged. Its positive charges are distributed on the pyridine N atoms, as well as the Cl^- ions used to balance the charges just exist in the pores of the 3D supramolecular structure in the free form.

2.2 PXRD and TGA

TGA and PXRD were used for thermal and chemi-

cal stability analysis. The phase purity of CP **1** was confirmed by the PXRD pattern. The peaks of the synthesized sample matched well with the simulated results generated from single-crystal diffraction data, suggesting that the crystal of **1** was pure (Fig. 2). To testify to the pH and water stability of **1**, the corresponding measurements were performed at ambient temperature, in which the ground samples of **1** were treated with different pH-value solutions (pH=7 and 10) or purified water, and immersed for 3 d, respectively. The results display that the main diffraction peaks of **1** treated under different pH-value solutions or purified water coincide with those of the initially synthesized sample, indicating that **1** had excellent stability in water (Fig. 2). The stability of **1** in water is a necessary condition for it to be used as an aqueous phase detection material.

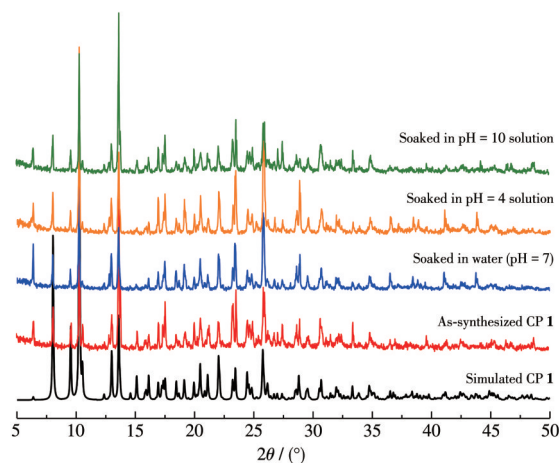


Fig. 2 PXRD patterns of CP **1**

The thermal stability of CP **1** was studied under an N_2 atmosphere from 20 to $800\text{ }^\circ\text{C}$ (Fig. 3). The TG

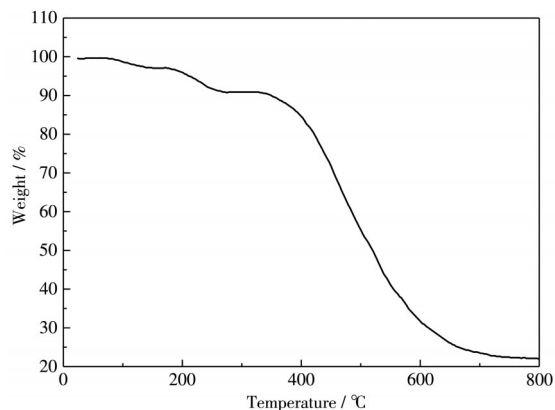


Fig. 3 TG curve of CP **1**

curve showed a weight loss of 3.25% from 80 to 170 °C, which is attributed to the loss of the two uncoordinated free water. With further being heated, **1** lost weight about 4.76% from about 180 to 310 °C, which could be mainly ascribed to the loss of the three coordinated water. After 380 °C, the crystal structure began to collapse due to the decomposition of organic ligands, indicating that **1** has good stability.

2.3 Photoluminescence properties

The solid luminescence properties of ligand (H₂L)Cl₂ and CP **1** have been investigated at room temperature as shown in Fig. 4. The free ligand (H₂L)Cl₂ showed a wide emission peak at 472 nm ($\lambda_{\text{ex}}=416$ nm),

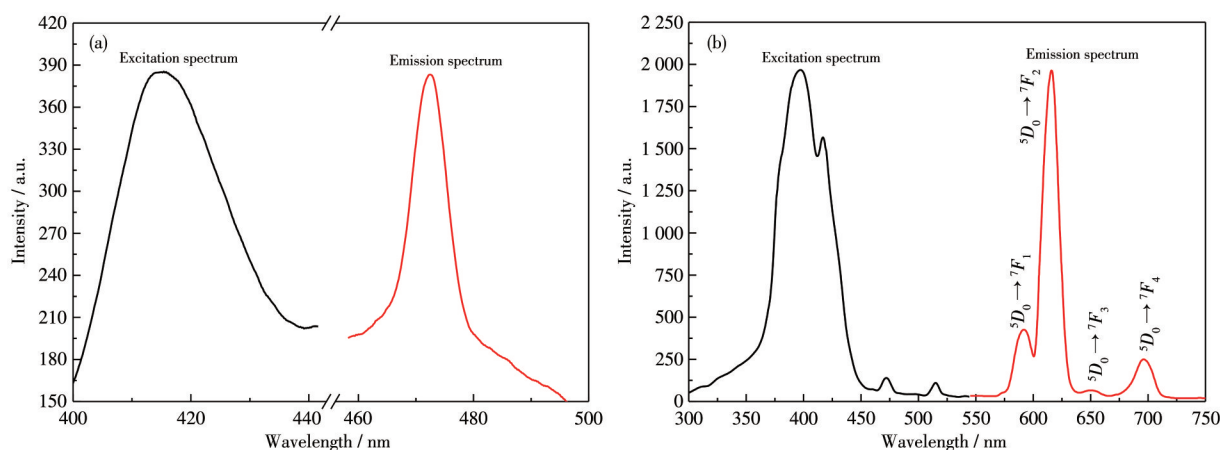


Fig. 4 Solid-state luminescent spectra of free ligand (H₂L)Cl₂ (a) and CP **1** (b)

2.4 Selective detection of furacilin

Because of the excellent water stability and strong fluorescence of CP **1**, the application in detecting eight daily common antibiotics in water systems was explored. First, the sensing ability of **1** toward different antibiotics was investigated by adding 100 $\mu\text{mol}\cdot\text{L}^{-1}$ aqueous solutions of gentamicin (GEN), kanamycin (KAN), penicillin (PEN), cefixime (CFX), cefradine (CED), furacilin (FAC), roxithromycin (ROX), and azithromycin (AZM) to suspensions of **1** (Fig. 5a). Sensing experiments showed that among all antibiotics studied in this work, FAC showed a significant quenching effect on the luminescence intensity of **1**, while other antibiotics showed a smaller quenching effect (Fig. 5b). Hence, the preliminary sensing experiments revealed that **1** was capable of sensing FAC most selectively.

To further understand the ability of CP **1** to detect

which is assigned to the typical $\pi^* - \pi$ transition of ligands^[15-16]. The sample of **1** exhibited emission peaks of typical Eu(III) ions at 590, 616, 650, and 695 nm ($\lambda_{\text{ex}}=397$ nm), which belong to $^5D_0 \rightarrow ^7F_1$, $^5D_0 \rightarrow ^7F_2$, $^5D_0 \rightarrow ^7F_3$, and $^5D_0 \rightarrow ^7F_4$ transitions of Eu³⁺ ions, respectively. Notably, there was no emission band of the ligand observed in the emission spectra of the compounds, indicating the efficient energy transfer from the ligand to the Eu³⁺ ion. These results indicate that ligand (H₂L)Cl₂ is an excellent antenna chromophore for sensitizing Eu³⁺ ions, which means that the energy transfers from the ligand to the Eu³⁺ center effectively^[16].

FAC, we continued to study the fluorescence titration obtained by adding different concentrations of FAC to **1** - suspension (in water) to explore the relationship between FAC concentration and the fluorescence intensity. As shown in Fig. 5c, when FAC was gradually added to **1** - suspension, the fluorescence intensity decreased with the increase of FAC concentration. By measuring the fluorescence intensity at 616 nm, we found that the decrease in fluorescence intensity was particularly obvious. When FAC concentration reached 80 $\mu\text{mol}\cdot\text{L}^{-1}$, the fluorescence of **1** - suspension was almost extinguished by 90%. Hence, we used the calculated I_0/I as the ordinate and the FAC concentration ($\mu\text{mol}\cdot\text{L}^{-1}$) as abscissa, to draw the result, as shown in Fig. 5d. We found that the fluorescence quenching efficiency of FAC in a concentration range from 5 to 44 $\mu\text{mol}\cdot\text{L}^{-1}$ conformed to the Stern-Volmer (SV) linear

fitting formula: $I_0/I=1+K_{SV}c_{FAC}$, where I_0 is the initial fluorescence intensity of **1**-suspension without FAC, I is the fluorescence intensity of **1**-suspension after adding FAC, and c_{FAC} is the concentration of FAC added. After calculation, the quenching constant K_{SV} was $5.198 \times 10^4 \text{ L} \cdot \text{mol}^{-1}$ in the low FAC concentration range ($R^2=0.9969$), which corresponded to the highest known

value of CP - based sensors previously reported^[21-26] (Table 4). At the same time, the limit of detection (LOD) was calculated by $3\sigma/K$, where σ is the standard error and K is the slope obtained by linear fitting of concentration-dependent luminescence intensity at low concentration. The LOD value of **1** for FAC was found to be $0.13 \mu\text{mol} \cdot \text{L}^{-1}$. This demonstrates the potential of

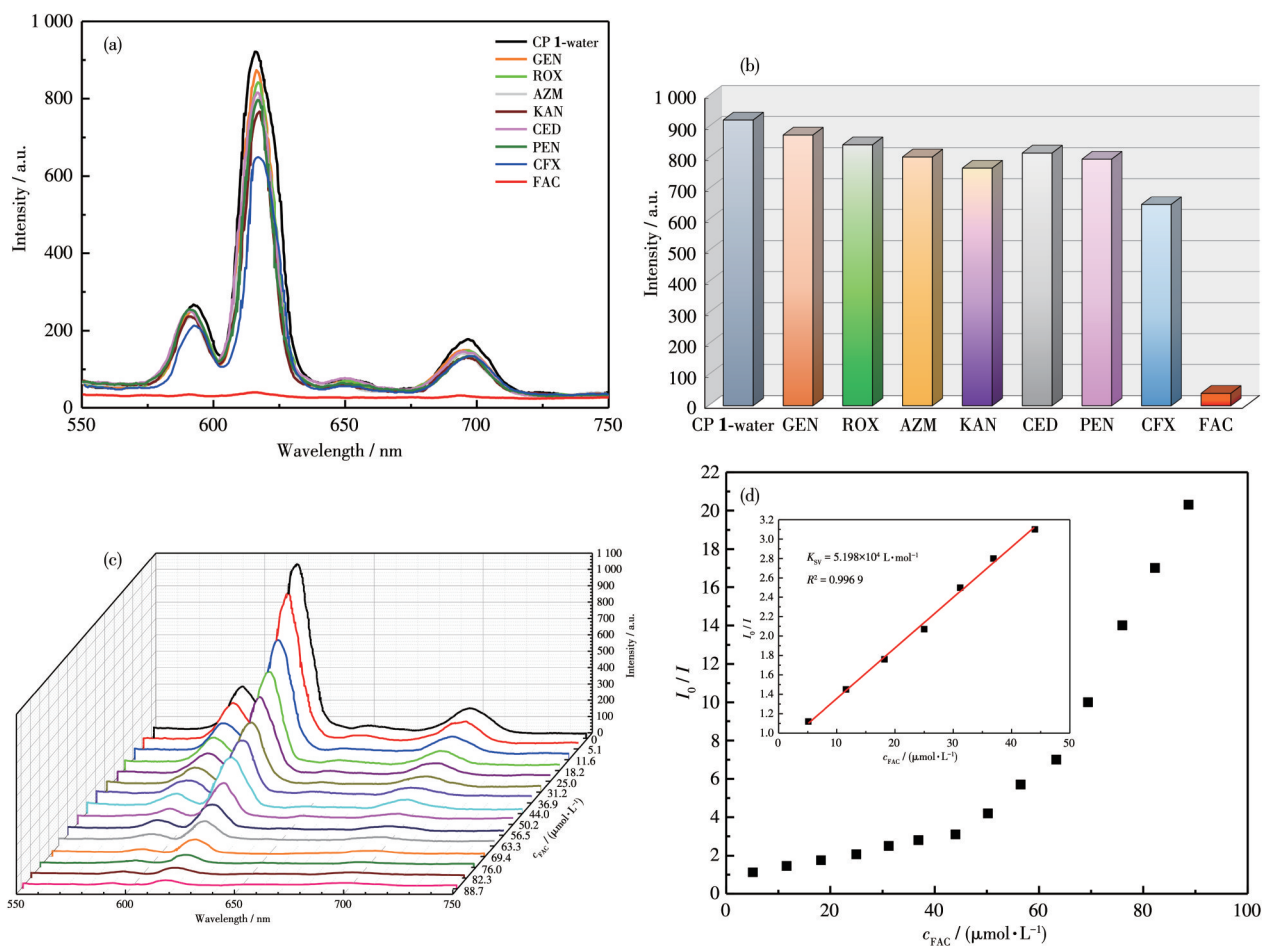


Fig.5 (a) Emission spectra of **1** adding $100 \mu\text{mol} \cdot \text{L}^{-1}$ aqueous solutions of different antibiotics; (b) Comparisons of the luminescence intensity of **1**-suspension in different common antibiotics; (c) Luminescence spectra of **1**-suspension titrated by adding different concentrations of FAC; (d) SV plot of **1** quenched by FAC in water

Table 4 Comparison of K_{SV} and LOD values for CPs reported for aqueous phase sensing of furacilin

CP-based sensor	$K_{SV} / (\text{L} \cdot \text{mol}^{-1})$	LOD / ($\mu\text{mol} \cdot \text{L}^{-1}$)	Ref.
$(\text{Me}_2\text{NH}_2)[\text{Zn}(\text{NH}_2\text{-TCB})]$	4.85×10^4	0.30	[21]
$[\text{Zn}(\text{L})_2] \cdot \text{CH}_2\text{Cl}_2 \cdot \text{CH}_3\text{OH}$	1.62×10^4	1.21	[22]
$[\text{CdL}_4]\text{CB}$	4.01×10^4	0.45	[23]
$\text{Zn}_6\text{Yb}_3\text{L}_5(\text{HL})(\text{NO}_3)_4(\text{DMF})_6(\text{EtOH})_4(\text{H}_2\text{O})_4$	2.70×10^4	86	[24]
$[\text{Cd}_3(\text{L})_3(\text{DMA})_4] \cdot 2\text{DMA} \cdot 4\text{H}_2\text{O}$	2.915×10^4	0.22	[25]
$[\text{Cd}(\text{tib})_2](\text{NO}_2)_2 \cdot 0.5\text{DMA} \cdot \text{H}_2\text{O}$	2.95×10^4	0.56	[26]
CP 1	5.198×10^4	0.13	This work

1 as a highly sensitive luminescent probe for FAC.

To further detect the application of CP **1** sensor in a biological system, we carried out the sensing experiment of **1** in 2-(4-(2-hydroxyethyl)piperazin-1-yl)ethanesulfonic acid (HEPES) simulated physiological environment ($20 \mu\text{mol}\cdot\text{L}^{-1}$ HEPES aqueous buffer solution, $\text{pH}=7$)^[30-32]. We found that the fluorescence intensity in this simulated physiological environment was the same as that in pure aqueous solution; At the same time, we also selected FAC with a concentration of $50 \mu\text{mol}\cdot\text{L}^{-1}$ as the representative to investigate the fluorescence intensity of **1** in water and the simulated physiological environment. The intensity did not change significantly (Fig.6). This indicates that the fluorescence sensing of **1** to FAC may be of great use in physiology.

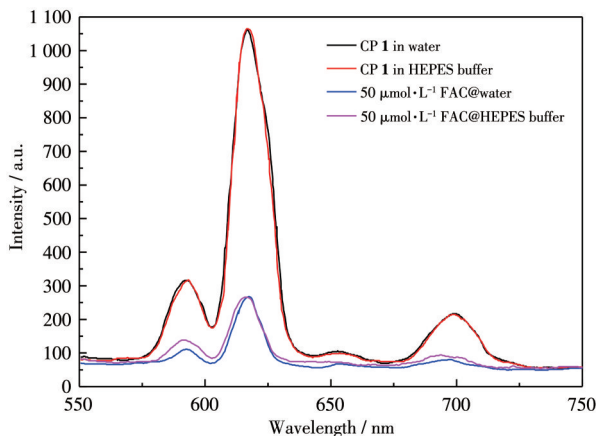


Fig.6 Emission spectra of **1** after immersing in HEPES aqueous buffer solution or pure water

In addition, considering that the reproducibility of the chemical sensor is an important parameter of practicability, the repeatability of CP **1** fluorescence detection was also studied. It is found that **1** can be reused at least five times after multiple dispersion, crystallization, and centrifugal washing in water. By monitoring the emission spectrum of **1**-suspension in the presence of $100 \mu\text{mol}\cdot\text{L}^{-1}$ FAC, it was found that the quenching efficiency of each cycle was substantially unchanged (Fig.7). Additionally, it is important to investigate the luminescence quenching mechanism and selective detection ability of **1**. The PXRD pattern of **1** recovered after five detection cycles showed almost the same as the initial sample, indicating the high stability of the material (Fig.8a). Then, by testing the FT-IR spectrum

after five cycles, we found that the main spectrum (3 424(br), 1 609(s), 1 564(s), 1 446(w), 1 385(s), 1 237(m), 1 121(m), 1 077(m), 1 043(m)) of **1** was also consistent with that of the original synthesized sample. In addition, an ICP experiment was also performed to monitor the release of Eu(III) ions from **1** after five cycles of sensing experiments. The mass concentration of Eu(III) ion in the filtrate was $0.17 \mu\text{g}\cdot\text{mL}^{-1}$, which

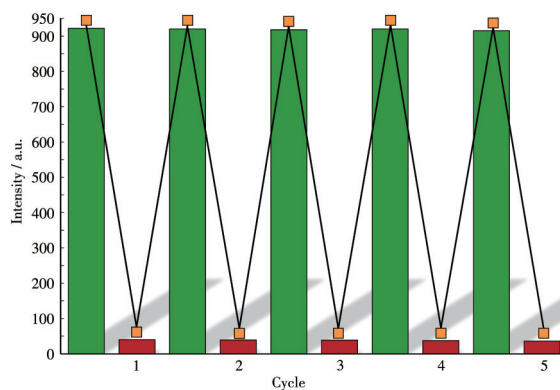


Fig.7 Quenching cycle test of **1** after adding $100 \mu\text{mol}\cdot\text{L}^{-1}$ FAC in aquatic system

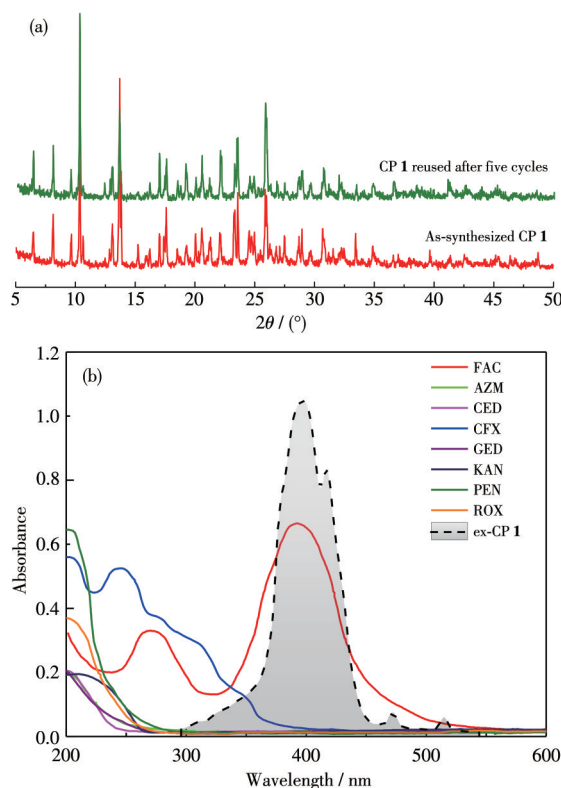


Fig.8 (a) PXRD patterns of **1** after detection of FAC for five cycles; (b) Spectral overlap between the UV-Vis spectra of the antibiotics in aqueous solution and the excitation spectrum of **1**

was close to that of the blank sample ($0.14 \mu\text{g}\cdot\text{mL}^{-1}$). This ICP test result showed that there was no release of Cd(II) ions from the samples of **1** in the sensing experiments. Combining the XRD, FT-IR, and ICP results after five cycles, we find that the luminescence quenching is not induced by the framework collapse and **1** can be reused as a probe.

Then, the inner filter effects (IFE) can be used to explain the quenching effects. As shown in Fig. 8b, there was a significant spectral overlap between the absorption band of FAC and the excitation spectrum of **1**; however, there was no effective overlap for other antibiotics, indicating that there exists the competitive absorption of the excitation energy between **1** and the antibiotics analytes. The above results show that **1** can be used as a fluorescent probe for FAC and has high selectivity, high sensitivity, and reusability.

3 Conclusions

A novel Eu(III) coordination polymer (**1**) was synthesized under hydrothermal conditions by a zwitterionic organic ligand. X-ray diffraction analysis shows **1** has a cationic skeleton on the main network. Firstly, the solid-state luminescence properties of **1** were investigated, realizing the zwitterionic ligand is an excellent antenna chromophore for sensitizing Eu^{3+} ions. In addition, this water-stable **1** was utilized as a chemosensor to detect various common antibiotics to find that this complex can exhibit high selectivity, sensitivity, and recyclability in the detection of furacilin molecules in aqueous phases. Our laboratory is also carrying out follow-up research work.

References:

- [1]Luz I, Soukri M, Lail M. Flying MOFs: Polyamine-containing Fluidized MOF/SiO₂ Hybrid Materials for CO₂ Capture from Post-combustion Flue Gas. *Chem. Sci.*, **2018**,**9**(20):4589-4599
- [2]Ding M L, Flaig R W, Jiang H L, Yaghi O M. Carbon Capture and Conversion Using Metal-Organic Frameworks and MOF-Based Materials. *Chem. Soc. Rev.*, **2019**,**48**(10):2783-2828
- [3]Ahmad M S, Khalid M, Khan M S, Shahid M, Ahmad M. Ni(II)-Based One Dimensional Coordination Polymers for Environmental Remediation: Design, Topology, Magnetism and the Selective Adsorption of Cationic Dyes. *CrystEngComm*, **2021**,**23**(36):6253-6266
- [4]王晓晴, 马学慧, 冯豆豆, 唐婧, 吴丹. 一种水稳性的 Zn 基金属-有机框架的合成及其对铁离子及 2,6-二氯-4-硝基苯胺的荧光识别. *无机化学学报*, **2022**,**38**(1):137-144
- WANG X Q, MA X H, FENG D D, TANG J, WU D. Synthesis of a Water-Stable Zn(II)-Based Metal-Organic Framework for Luminescence Detecting Fe^{3+} and 2,6-Dichloro-4-nitroaniline. *Chinese J. Inorg. Chem.*, **2022**,**38**(1):137-144
- [5]Liu J T, Huang J, Zhang L, Lei J P. Multifunctional Metal-Organic Framework Heterostructures for Enhanced Cancer Therapy. *Chem. Soc. Rev.*, **2021**,**50**(2):1188-1218
- [6]Huangfu M J, Wang M, Lin C, Wang J, Wu P Y. Luminescent Metal-Organic Frameworks as Chemical Sensors Based on "Mechanism-Response": A Review. *Dalton Trans.*, **2021**,**50**(10):3429-3449
- [7]Yi F Y, Chen D X, Wu M K, Han L, Jiang H L. Emerging Porous Nanosheets: From Fundamental Synthesis to Promising Applications. *ChemPlusChem*, **2016**,**81**(8):675-690
- [8]潘兆瑞, 郑和根. 2-(5-甲基-1,3,4-噻二唑)-硫乙酸锌(II)配合物的合成、晶体结构和性质. *无机化学学报*, **2017**,**33**(9):1678-1684
- PAN Z R, ZHENG H G. Syntheses, Crystal Structures and Properties of 2-(5-Methyl-1,3,4-thiadiazol-2-ylthio Zinc(II) Coordination Compounds. *Chinese J. Inorg. Chem.*, **2017**,**33**(9):1678-1684
- [9]Xu J L, Xu Y H, Bu X H. Advances in Emerging Crystalline Porous Materials. *Small*, **2021**,**17**(22):2102331
- [10]Chen Z Y, Meng G Y, Tang H J, Ye Y C, Sun R Y, Chen M X, Wang K M. A Novel Cationic Iridium(III) Complex with a Thiorhodamine-Based Auxiliary Ligand: Application for Luminescent and Colorimetric Detection of Hg^{2+} in an Aqueous Solution. *New J. Chem.*, **2017**,**41**(16):8312-8319
- [11]Li G, Liu W S, Yang S L, Zhang L, Bu R, Gao E Q. Anion-Afforded Functions of Ionic Metal-Organic Frameworks: Ionochromism, Anion Conduction, and Catalysis. *Inorg. Chem.*, **2022**,**61**(2):902-910
- [12]刘进剑, 刘娜, 陆艺炜, 赵国政. 基于紫精组分构筑的三种光致变色共晶体. *无机化学学报*, **2021**,**37**(5):937-944
- LIU J J, LIU N, LU Y W, ZHAO G Z. Three Photochromic Co-crystals Based on Viologen Moiety. *Chinese J. Inorg. Chem.*, **2021**,**37**(5):937-944
- [13]Liu X Y, Yin X M, Yang S L, Zhang L, Bu R, Gao E Q. Chromic and Fluorescence-Responsive Metal-Organic Frameworks Afforded by N-Amination Modification. *ACS Appl. Mater. Interfaces*, **2021**,**13**(17):20380-20387
- [14]Zhang X, Sun J, Wei G F, Liu Z P, Yang H M, Wang K M, Fei H H. *In Situ* Generation of an N-Heterocyclic Carbene Functionalized Metal-Organic Framework by Postsynthetic Ligand Exchange: Efficient and Selective Hydrosilylation of CO₂. *Angew. Chem. Int. Ed.*, **2019**,**58**(9):2844-2849
- [15]Zhao X Y, Liang B, Xiong K C, Shi Y W, Yang S L, Wei T Y, Zhang H, Zhang Q F, Gai Y L. Two Novel Lead-Based Coordination Polymers for Luminescence Sensing of Anions, Cations and Small Organic Molecules. *Dalton Trans.*, **2020**,**49**(17):5695-5702
- [16]Wang K M, Du L, Ma Y L, Zhao J S, Wang Q, Yan T, Zhao Q H. Multifunctional Chemical Sensors and Luminescent Thermometers

- Based on Lanthanide Metal-Organic Framework Materials. *CrystEngComm*, **2016**,**18**(15):2690-2700
- [17] Yu M K, Xie Y, Wang X Y, Li Y X, Li G M. Highly Water-Stable Dye@Ln-MOFs for Sensitive and Selective Detection toward Antibiotics in Water. *ACS Appl. Mater. Interfaces*, **2019**,**11**(23): 21201 - 21210
- [18] Yue X Y, Zhou Z J, Li M, Jie M S, Xu B C, Bai Y H. Inner-Filter Effect Induced Fluorescent Sensor Based on Fusiform Al - MOF Nanosheets for Sensitive and Visual Detection of Nitrofurantoin in Milk. *Food Chem.*, **2020**,**367**:130763
- [19] Wang B, Liu J H, Yu J M, Lv J, Dong C, Li J R. Broad Spectrum Detection of Veterinary Drugs with a Highly Stable Metal -Organic Framework. *J. Hazard. Mater.*, **2020**,**382**:121018
- [20] Xu S, Shi J J, Ding B, Liu Z Y, Wang X G, Zhao X J, Yang E C. A Heterometallic Sodium (I) - Europium (III) - Organic Layer Exhibiting Dual - Responsive Luminescent Sensing for Nitrofurantoin Antibiotics, $\text{Cr}_2\text{O}_7^{2-}$ and MnO_4^- Anions. *Dalton Trans.*, **2019**,**48**(5):1823-1834
- [21] Fan L, Zhao D S, Zhang H H, Wang F, Li B, Yang L L, Deng Y X, Zhang X T. A Hydrolytically Stable Amino - Functionalized Zinc (II) Metal -Organic Framework Containing Nanocages for Selective Gas Adsorption and Luminescent Sensing. *Microporous Mesoporous Mater.*, **2021**,**326**:111396
- [22] Liu Y, Zhao Y, Liu Z Q, Liu X H, Zhang X D, Sun W Y. Coordination Polymers with Salicylaldehyde Ligands: Structural Diversity, Selective Sorption and Luminescence Sensing Properties. *CrystEngComm*, **2020**,**22**(2):304-310
- [23] Shi L L, Liu M, Fang C, Zhu X F, Li H. A Cucurbit[6]uril - Based Supramolecular Assembly Test Strip for Immediate Detection of Nitrofurantoin Antibiotics in Water. *CrystEngComm*, **2020**,**22**(44):7660-7667
- [24] Chen Y, Yang X P, Cheng Y B, Zhang L J, Yang Z, Schipper D. Regulated Detection of Antibiotics Based on a Near-IR - Luminescent Tubelike Zn(II) - Yb(III) Nanocluster. *Inorg. Chem.*, **2022**,**61**(2):1011-1017
- [25] Lu L Y, Tao X W, Chen F, Cheng A L, Xue Q S, Gao E Q. A Series of New Sulfone - Functionalized Coordination Polymers: Fascinating Architectures and Efficient Fluorescent Sensing of Nitrofurantoin Antibiotics. *J. Solid State Chem.*, **2021**,**301**:122251
- [26] Li B, Lei Q J, Wang F, Zhao D S, Deng Y X, Yang L L, Fan L M, Zhang Z G. A Stable Cationic Cd(II) Coordination Network as Bifunctional Chemosensor with High Sensitivity and Selective Detection of Antibiotics and Cr(VI) Anions in Water. *J. Solid State Chem.*, **2021**, **298**:122117
- [27] Sheldrick G M. Crystal Structure Refinement with SHELXL. *Acta Crystallogr. Sect. C*, **2015**,**C71**:3-8
- [28] Spek A L. PLATON SQUEEZE: A Tool for the Calculation of the Disordered Solvent Contribution to the Calculated Structure Factors. *Acta Crystallogr. Sect. C*, **2015**,**C71**:9-18
- [29] Dolomanov O V, Bourhis L J, Gildea R J, Howard J A K, Puschmann H. OLEX2: A Complete Structure Solution, Refinement and Analysis Program. *J. Appl. Cryst.*, **2009**,**42**:339-341
- [30] Liu L Z, Wang Y, Lin R Y, Yao Z Z, Lin Q J, Wang L H, Zhang Z J, Xiang S C. Two Water - Stable Lanthanide Metal - Organic Frameworks with Oxygen - Rich Channels for Fluorescence Sensing of Fe(III) Ions in Aqueous Solution. *Dalton Trans.*, **2018**,**47**(45):16190-16196
- [31] Wu P Y, Xia L L, Huangfu M J, Fu F B, Wang M Q, Wen B X, Yang Z Y, Wang J. Lanthanide - Based Metal - Organic Frameworks Containing "V - Shaped" Tetracarboxylate Ligands: Synthesis, Crystal Structures, "Naked - Eye" Luminescent Detection, and Catalytic Properties. *Inorg. Chem.*, **2020**,**59**(1):264-273
- [32] Dang S, Ma E, Sun Z M, Zhang H J. A Layer - Structured Eu - MOF as a Highly Selective Fluorescent Probe for Fe^{3+} Detection through a Cation - Exchange Approach. *J. Mater. Chem.*, **2012**,**22**(33):16920-16926